VNU Journal of Science: Mathematics – Physics, Vol. 35, No. 3 (2019) 98-106

VNU Journal of Science: Mathematics - Physics

Journal homepage: https://js.vnu.edu.vn/MaP

Original Article

Optical Simulation of Planar $CH_3NH_3PbI_3$ Perovskite Solar Cells

Nguyen Duc Cuong[1,*]

Faculty of Engineering Physics and Nanotechnology, VNU University of Engineering and Technology, 144 Xuan Thuy, Cau Giay, Hanoi, Vietnam

Received 08 May 2019
Revised 24 May 2019; Accepted 30 May 2019

Abstract: In this work, optical simulation results of planar $CH_3NH_3PbI_3$ solar cells using a MATLAB script developed by McGehee's group (Stanford University) are presented. The device structure is of FTO/HEL/AL/ETL/LiF/Al, where HEL is the hole-extraction layer, AL is the active layer ($CH_3NH_3PbI_3$), and EEL is the electron-extraction layer. In this MATLAB script, the transfer matrix method was used, where transmission and reflection were calculated for each interface in the stack as well as attenuation in each layer. The wavelength-dependent optical constants (*n* and *k*) of each layer were measured by spectroscopic ellipsometry (SE). The exciton generation rates within the active layer were calculated based on data of optical constants, as well as the thickness of each layer. Considering the Internal Quantum Efficiency (IQE) equal to 100% at all wavelengths, the predicted short-circuit currents (J_{SC}) were also estimated. The obtained results show a good agreement with the experimental values of J_{SC} measured on real devices.

Keywords: planar solar cells, $CH_3NH_3PbI_3$ perovskite, optical simulations, spectroscopic ellipsometry.

1. Introduction

In recent years, perovskite solar cells have been attracting much attention due to their ease of processing, low cost, and high Power Conversion Efficiency (PCE). The PCE of perovskite solar cells based on the methylammonium lead iodide $CH_3NH_3PbI_3$ (shortly as $MAPbI_3$) has increased from 3.8% in 2009 [1] to 19.2% in 2017 [2]. The PCE of multi-layer solar cells in general and planar perovskite solar cells, in particular, is strongly varied depending not only on the optical and electrical properties

*Corresponding author.
Email address: cuonghd93@gmail.com

https//doi.org/ 10.25073/2588-1124/vnumap.4349

of active layers as well as charge transport layers but also on the device structure, i.e. the thickness of each layer. A high exciton generation rate, i.e. number of electron-hole pairs generated in a unit of time and a unit of volume of the active layer is a crucial factor for a highly efficient solar cell. Therefore, optical simulation steps help to find optimized structures for solar cells devices and to reduce the cost of trial and error experiments.

In this paper, optical simulations using a MATLAB script developed by McGehee's group (Stanford University) [3], [4] were performed on planar multi-layer perovskite solar cells, utilizing PEDOT:PSS (CLEVIOS P VP AI 4083) and Cu-doped NiO_x (Cu:NiO_x) as hole-extraction layers (HEL), $CH_3NH_3PbI_3$ ($MAPbI_3$) as an active layer (AL) and PCBM as an electron-extraction layer (EEL). In this MATLAB script, the transfer matrix method was used, where transmission and reflection were calculated for each interface in the stack as well as attenuation in each layer, based on optical constants of individual materials [5], [6]. The wavelength-dependent optical constants (*n* and *k*) of each layer were measured by spectroscopic ellipsometry (SE) [7]. Briefly, by the SE, the change in polarized light upon light reflection on a sample (or light transmission by a sample) was measured at different wavelengths. Amplitude ratio ψ and phase difference Δ between p-and s-polarized light waves were obtained directly from the measurement, and then optical constants (*n* and *k*) were found by using an optical model relevant to the sample.

The exciton generation rates within layer *j* were calculated according to [5]:

$$G_j(x,\lambda) = \frac{\lambda}{hc} Q_j(x,\lambda) \tag{1}$$

where $Q_j(x,\lambda) = \frac{4\pi c \varepsilon_0 n_j k_j}{2\lambda} \left|E_j(x,\lambda)\right|^2$ is the time average of the energy dissipated per second in layer *j* at position *x* at normal incidence, *c* is the speed of light, ε_0 is the permittivity of free space and $E_j(x,\lambda)$ is internal optical electric field.

Considering the Internal Quantum Efficiency (IQE) equal to 100% at all wavelengths, the predicted J_{SC} also can be calculated according to:

$$J_{\text{SC-predicted}} = e\iint G_{AL}(x,\lambda)\, d\lambda dx \tag{2}$$

where $G_{AL}(x,\lambda)$ is the exciton generation rate within the active layer.

2. Experimental

The FTO-coated glass (7.33 $\Omega \cdot sq^{-1}$) substrates were patterned by Zn powder and HCl acid (35%) and cleaned by detergent and successive ultrasonic treatment in acetone, isopropanol before drying under nitrogen flow. Right before deposition of hole-extraction layer (HEL), the FTO-coated glass substrates were treated by UV-ozone for 30 min.

PEDOT:PSS (CLEVIOS P VP AI 4083) was filtered through a 0.45 μm PVDF filter before casting on patterned FTO-coated glass substrates. Spin-coating at 3,000 rpm for 60 s and annealing at 150 °C for 20 min in air produced a 40 nm thick PEDOT:PSS layer.

The Cu-doped NiO_x HEL were deposited by spin-coating respective precursor on pre-cleaned FTO substrates at 4,000 rpm for 30 s, followed by annealing at 550 °C for 30 min in air. The thickness of Cu-doped NiO_x measured by spectroscopic ellipsometry was 15.06±0.07 nm. Right before deposition of active layers (ALs), the FTO/Cu:NiO_x substrates were treated by UV-ozone for 10 min.

$CH_3NH_3PbI_3$ ($MAPbI_3$) layer was formed on FTO/HEL substrates by a single-step method with non-solvent dripping [8]. PbI_2 and MAI were dissolved in a mixture solvent of GBL and DMSO (7:3 v/v) at a concentration of 1.1 M under stirring at 60 °C for 12 h. The resulting solution was coated onto the FTO/HEL substrates by a consecutive two-step spin-coating process at 1,000 and 5,000 rpm for 10 and 20 s, respectively. During the second spin-coating step (at the eleventh second), the substrate (3 cm × 3 cm) was treated with 0.6 ml of non-solvent (toluene, *p*-xylene or chlorobenzene) drop-casting. Right after the spin-coating process, the films were transparent and colorless, corresponding to the MAI-PbI_2-DMSO intermediate phase. The substrate was then dried on a hot plate at 100 °C for 10 min. All these steps were performed in a N_2-filled glove box. The resulting films were semi-transparent with dark-brown color, indicating the formation of the perovskite phase with good crystalline quality.

A solution of Phenyl-C61-butyric acid methyl ester (PCBM) in chlorobenzene (20 mg/ml) was spin-coated on the FTO/HEL/$MAPbI_3$ substrate at 1000 rpm for 30 s, followed by annealing at 110 °C for 10 min in a N_2-filled glove box.

Finally, 0.5 nm of LiF and 120 nm of Al were subsequently deposited by thermal evaporation under a 2.4×10^{-6} Torr vacuum on top of the devices to form the back contacts. A shadow mask was used to define a 2×2 array of 0.4×0.6 cm^2 rectangular contacts. The solar cells were then hermetically encapsulated with glass cover using an ultraviolet-curable epoxy sealant (XNR5570-A1 NAGASE ChemTex), with an ultraviolet exposure of 2 min.

Absorbance spectra were taken by a Jasco V670 UV-Vis-NIR spectrophotometer equipped with an integrating sphere.

Thin films for SE measurements were prepared on Si/SiO_2 substrates following the same recipes mentioned above. SE spectra were measured by a V-VASE Ellipsometer (J. A. Woollam) and analyzed by CompleteEASE Software (version 5.01, J. A. Woollam) [9].

Side-view Scanning Electron Microscopy (SEM) image was taken from a Hitachi ultrahigh-resolution/SEM S-4800 scanning electron microscope.

3. Results and discussion

Figure 1 shows the wavelength-dependent spectra of the two ellipsometry parameters (ψ, Δ) and respective optical constants (n, k) of a $MAPbI_3$ thin film formed on Si/SiO_2 substrate. Here the fitting procedure according to the Cauchy optical model yielded not only optical constants (n, k), but also the thickness of 178.656±0.199 nm of the $MAPbI_3$ thin film with a mean-squared error (MSE) of 4.881. A closer look at the extinction coefficient (k) spectrum revealed that the onset is observed at around 760 nm, while a shoulder and a peak are observed at 480 nm and 360 nm, respectively [10], [11]. Those positions are totally consistent with the absorbance spectrum (dashed line) measured by a UV-Vis-NIR spectrometer. In addition, those positions are in good agreement with the previous report of Even et al., who pointed out that the broad light-harvesting abilities of the inorganic-organic family of perovskites $CH_3NH_3PbI_3$ are a direct consequence of their multi-bandgap and multi-valley nature [12].

Optical constants of other materials were obtained in a similar manner. **Figure 2** shows optical constants of FTO, PEDOT:PSS (CLEVIOS P VP AI 4083), Cu:NiO_x, $MAPbI_3$, and PCBM. The absorption coefficient (α) of $MAPbI_3$ estimated as 98522 cm^{-1} at 550 nm, according to the following relation:

$$\alpha = 4\pi k/\lambda \quad (3)$$

Tauc plot (i.e. $(\alpha h\nu)^2$ vs. $h\nu$) for direct bandgap materials shown in **Figure 3** reveals that the optical band gap of $MAPbI_3$ is 1.609 eV, that is slightly larger than the value obtained by theoretical calculations [13] but smaller than the value obtained by PL measurements [10], [11].

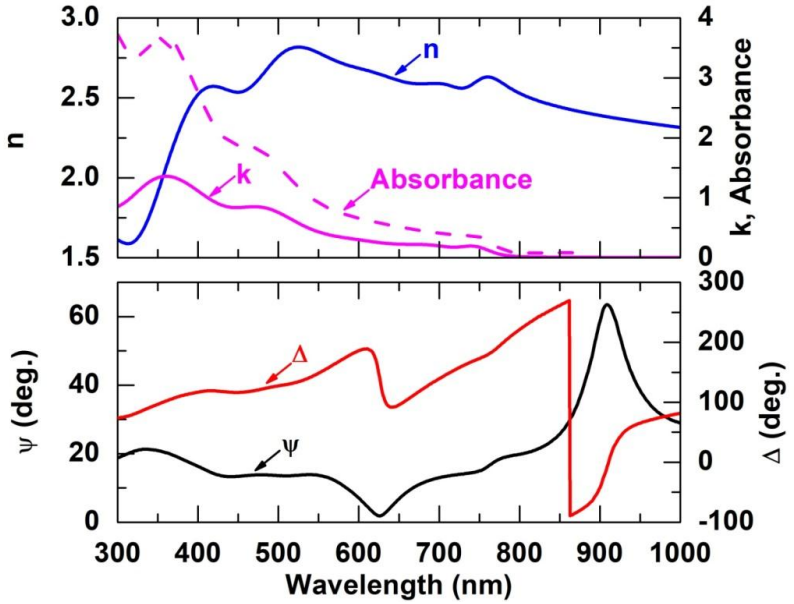

Figure 1. Wave-length dependent spectra of (ψ, Δ) and respective optical constants (n, k) obtained from a $MAPbI_3$ thin film formed on a Si/SiO_2 substrate. Absorbance spectrum (dashed line) measured by a UV-Vis-NIR spectrometer is also shown for comparison.

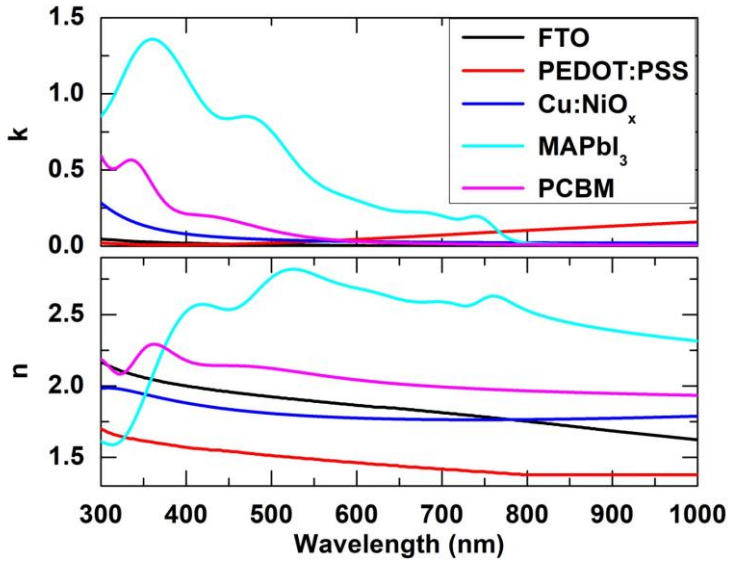

Figure 2. Wavelength-dependent optical constants (n, k) of FTO, PEDOT:PSS (CLEVIOS P VP AI 4083), $Cu:NiO_x$, $MAPbI_3$, and PCBM.

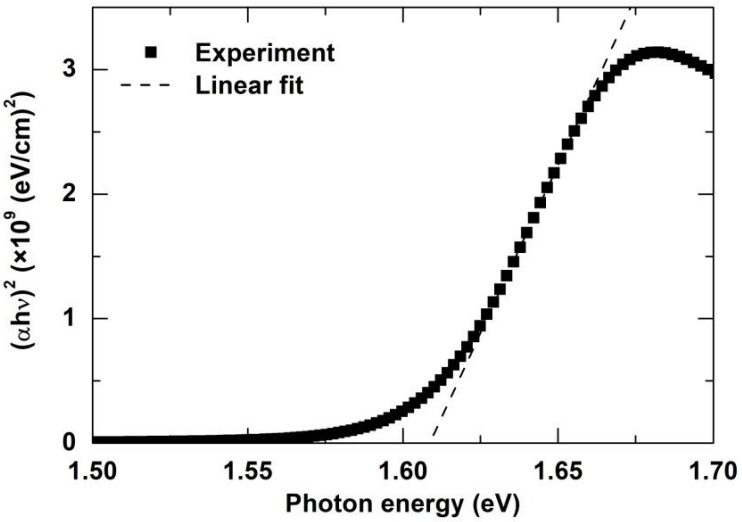

Figure 3. Tauc plot of $MAPbI_3$. Absorption coefficient (α) were estimated by $\alpha = 4\pi k/\lambda$ and extinction coefficient k was obtained from spectroscopic ellipsometry measurements (See **Figure 1**).

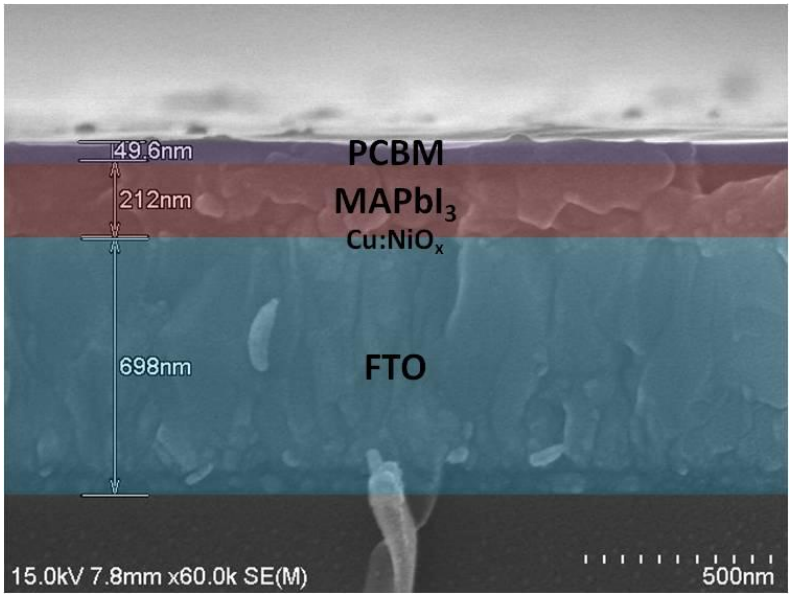

Figure 4. Side-view SEM image of FTO/Cu:NiO_x/$MAPbI_3$/PCBM stacked layers. Thicknesses of FTO (including Cu:NiO_x), $MAPbI_3$ and PCBM layers are 698, 212 and 49.6 nm, respectively. Cu:NiO_x layer (thickness of ~15 nm measured by SE) is too thin to be distinguished between FTO and $MAPbI_3$ layers.

Optical constants data of each material were then put into an Excel file, which serves as input data for the MATLAB script [3]. In addition, the names of materials which build the structure of the cell and their corresponding thickness (in nm) were also given in the script. According to the side-view SEM image (**Figure 4**), the thickness of each layer of the device can be exactly determined. The thickness of PEDOT:PSS of 40 nm were determined by an α-step instrument. Simulations were

performed with wavelength ranging from 300 to 1000 nm and the output data of the calculation includes internal optical electric field, exciton generation rate within the active layer, and predicted short-circuit current J_{SC}. With minor justification, the device structure of FTO(580 nm)/HEL/$MAPbI_3$(210 nm)/PCBM(50 nm)/LiF(0.5 nm)/Al(120 nm) were used as a standard. The position-dependent exciton generation rate within the $MAPbI_3$ active layer at various wavelengths $G_{AL}(x,\lambda)$ for two solar cells using PEDOT:PSS(40 nm) and Cu:NiO_x(15 nm) HELs are shown in **Figure 5**. In both cases, the maxima of $G_{AL}(x,\lambda)$ occur at the HEL/AL interface and wavelength of 450 nm, with the values of 6.046×10^{19} $s^{-1}\cdot cm^{-1}\cdot nm^{-1}$ and 6.147×10^{19} $s^{-1}\cdot cm^{-1}\cdot nm^{-1}$ for PEDOT:PSS-based and Cu:NiO_x-based devices, respectively. **Figure 6** shows the position-dependent exciton generation rate (obtained by integration by wavelengths varying from 300 nm to 1000 nm) within the $MAPbI_3$ active layer. Due to the lower absorption coefficient of Cu:NiO_x as compared to that of PEDOT:PSS (**Figure 2**), the exciton generation rate of Cu:NiO_x-based device is higher than that of PEDOT:PSS-based device over the whole active layer. Such distribution of generation rate requires long diffusion length of electron in $MAPbI_3$ material and good electron conductivity of EEL material to facilitate electron extraction at the cathode, and hence yield high J_{SC}. Fortunately, Xing et al. (2013) have discovered balanced long-range electron-hole diffusion lengths of at least 100 nanometers in solution-processed $MAPbI_3$ [11], which merely satisfies that requirement.

Based on the aforementioned standard device structure, the thickness of each layer was systematically varied. The dependence of predicted J_{SC} on the thickness of each layer is presented in **Figure 7**. Due to the same reason mentioned above, the reduction of $J_{SC\text{-predicted}}$ with the thickness of PEDOT is much faster than with thickness of Cu:NiO_x. As a result, $J_{SC\text{-predicted}}$ of PEDOT-based device is smaller than Cu:NiO_x-based device for most values of $MAPbI_3$ thickness (**Figure 7(c)**). Finally, although the PCBM layer is close to the back contact, it also has a noticeable impact on the $J_{SC\text{-predicted}}$ and causes $J_{SC\text{-predicted}}$ to reduce as $d_{PCBM} > 10$ nm (**Figure 7(d)**).

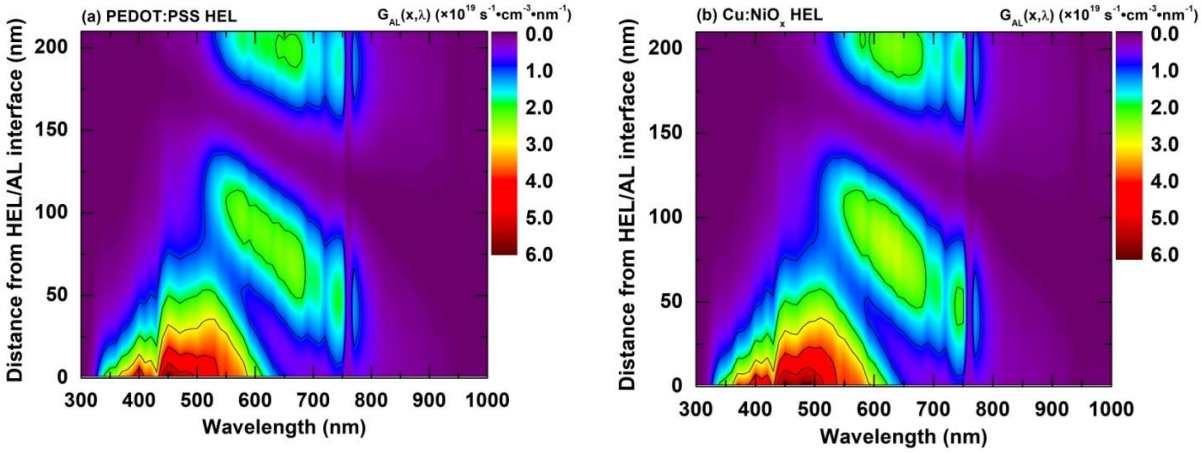

Figure 5. Position-dependent exciton generation rate at various wavelengths $G_{AL}(x,\lambda)$ (see Equation 1) within the $MAPbI_3$ active layer for planar solar cells with (a) PEDOT:PSS(40 nm) and (b) Cu:NiO_x(15 nm) HEL.

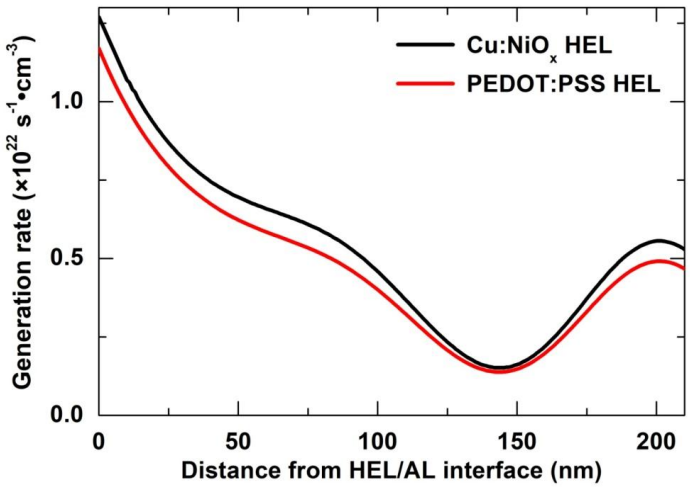

Figure 6. The variation of exciton generation rates within the $MAPbI_3$ AL with distance from HEL/AL interface for devices with PEDOT:PSS(40 nm) and Cu:NiO_x(15 nm) HELs.

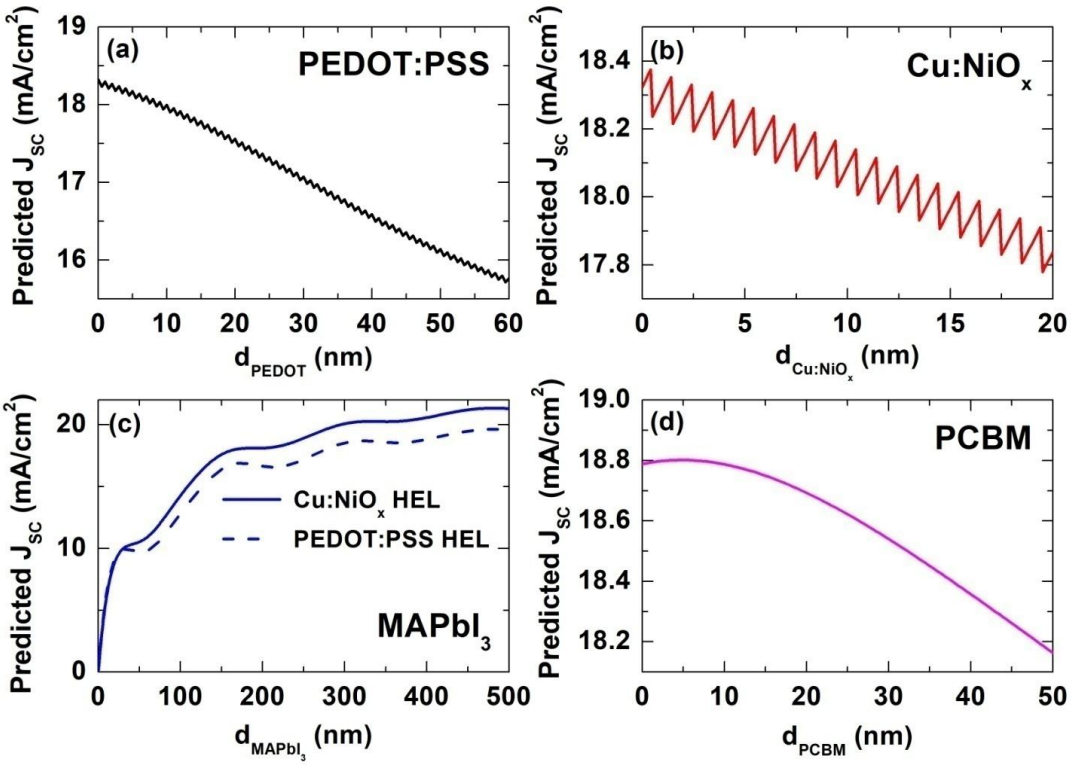

Figure 7. Dependence of predicted (maximum) $J_{SC\text{-predicted}}$ on the thickness of PEDOT:PSS, (b) Cu:NiO_x, (c) $MAPbI_3$ and (d) PCBM considering the Internal Quantum Efficiency (IQE) equal to 100% at all wavelengths.

Stacked device FTO(580 nm)/HEL/$MAPbI_3$(210 nm)/PCBM(50 nm)/LiF(0.5 nm)/Al(120 nm) with PEDOT:PSS(40 nm) and Cu:NiO_x(15 nm) HELs has predicted J_{SC} of 16.59 mA/cm^2 and 17.97 mA/cm^2, respectively. Interestingly, those values are in good agreement with the experimental data of J_{SC} ($J_{SC\text{-experimental}}$), which has been reported in [14]. The ratio between predicted and experimental J_{SC} is defined as:

$$\eta = \frac{J_{SC\text{-experimental}}}{J_{SC\text{-predicted}}} \quad (4)$$

The value of η estimated for PEDOT:PSS- and Cu:NiO_x-based devices are 95.24% and 100.78%, respectively. Considering the electron-extraction efficiencies at the PCBM side are identical for both devices, those values of η indicate that the hole-extraction efficiency Cu:NiO_x is better than PEDOT:PSS, that is crucial for the balance between electron and hole currents and hence high photocurrent.

4. Conclusions

In this work, optical simulations on planar $CH_3NH_3PbI_3$ perovskite solar cells using transfer matrix method were performed. The evaluated short-circuit currents showed a good agreement with the experimental data measured on real devices. As a result of those simulations, position-dependent exciton generation rates have been exactly determined and can serve as input data for the electrical simulation tools such as SCAPS [15]. It is worth to note that this method can be applied to all planar solar cells including organic solar cells, Si-based solar cells, and multi-junction solar cells.

Acknowledgements

This work has been supported by VNU University of Engineering and Technology under project number CN18.05. The author greatly appreciates Prof. Soonil Lee (Ajou University, Republic of Korea) for valuable comments and Dr. Sung-yoon Jo (KIST, Republic of Korea) for technical assistance in spectroscopic ellipsometry analyses.

References

[1] A. Kojima, K. Teshima, Y. Shirai, T. Miyasaka, Organometal halide perovskites as visible-light sensitizers for photovoltaic cells, J. Am. Chem. Soc. 131 (2009) 6050–6051. https://doi.org/10.1021/ja809598r.

[2] Y. Wu, F. Xie, H. Chen, X. Yang, H. Su, M. Cai, Z. Zhou, T. Noda, L. Han, Thermally stable $MAPbI_3$ perovskite solar cells with efficiency of 19.19% and area over 1 cm^2 achieved by additive engineering, Adv. Mater. 29 (2017) 1701073(1–8). https://doi.org/10.1002/adma.201701073.

[3] G.F. Burkhard, E.T. Hoke, Transfer matrix optical modeling, McGehee Group (Stanford Univ). 2011. Available online: http://web.stanford.edu/group/mcgehee/transfermatrix/index.html (accessed 10 October 2018).

[4] G.F. Burkhard, E.T. Hoke, M.D. McGehee, Accounting for interference, scattering, and electrode absorption to make accurate internal quantum efficiency measurements in organic and other thin solar cells. Adv. Mater., 22 (2010) 3293–3297. https://doi.org/10.1002/adma.201000883.

[5] L.A.A. Pettersson, L.S. Roman, O. Inganäs, Modeling photocurrent action spectra of photovoltaic devices based on organic thin films, J. Appl. Phys. 86 (1999) 487–496. https://doi.org/10.1063/1.370757.

[6] P. Peumans, A. Yakimov, S. Forrest, Small molecular weight organic thin-film photodetectors and solar cells, J. Appl. Phys. 93 (2003) 3693–3723. https://doi.org/10.1063/1.1534621.

[7] H. Fujiwara, Spectroscopic Ellipsometry : Principles and Applications, John Wiley & Sons, 2007.

[8] N.J. Jeon, J.H. Noh, Y.C. Kim, W.S. Yang, S.C. Ryu, S.I. Seok, Solvent engineering for high-performance inorganic–organic hybrid perovskite solar cells, Nat. Mater. 13 (2014) 897–903. https://doi.org/10.1038/nmat4014.

[9] CompleteEASE - J.A. Woollam. https://www.jawoollam.com/ellipsometry-software/completeease (accessed 15 September 2018).

[10] S.D. Stranks, G.E. Eperon, G. Grancini, C. Menelaou, M.J.P. Alcocer, T. Leijtens, L.M. Herz, A. Petrozza, H.J. Snaith, Electron-hole diffusion lengths exceeding 1 micrometer in an organometal trihalide perovskite absorber. Science 342, 2013, 341–344. https://doi.org/10.1126/science.1243982.

[11] G. Xing, N. Mathews, S. Sun, S.S. Lim, Y.M. Lam, M. Grätzel, S. Mhaisalkar, T.C. Sum, Long-range balanced electron- and hole-transport lengths in organic-inorganic $CH_3NH_3PbI_3$, Science 342 (2013) 344–347. https://doi.org/10.1126/science.1243167.

[12] J. Even, L. Pedesseau, C. Katan, Analysis of multi-valley and multi-bandgap absorption and enhancement of free carriers related to exciton screening in hybrid perovskites, J. Phys. Chem. C 118 (2014), 11566–11572. https://doi.org/10.1021/jp503337a.

[13] P. Umari, E. Mosconi, F. De Angelis, Relativistic GW calculations on $CH_3NH_3PbI_3$ and $CH_3NH_3SnI_3$ perovskites for solar cell applications, Sci. Rep. 4 (2014), 1–7. https://doi.org/10.1038/srep04467.

[14] D.C. Nguyen, S. Joe, N.Y. Ha, H.J. Park, J. Park, Y.H. Ahn, S. Lee, Hole-extraction layer dependence of defect formation and operation of planar $CH_3NH_3PbI_3$ perovskite solar cells, Phys. status solidi - Rapid Res. Lett. 11 (2016) 1600395(1–5). https://doi.org/10.1002/PSSR.201600395.

[15] A. Niemegeers, M. Burgelman, K. Decock, S. Degrave, V. Johan, SCAPS (a Solar Cell Capacitance Simulator). Available online: http://scaps.elis.ugent.be/SCAPSinstallatie.html (accessed 25 February 2019).